Synthesis of Large-Pore Methylene-Bridged Periodic Mesoporous Organosilicas and Its Implications

Xiao Ying Bao,[†] Xu Li,[‡] and X. S. Zhao*,[†]

Department of Chemical and Biomolecular Engineering, National University of Singapore, 10 Kent Ridge Crescent, Singapore 119620, and Institute of Materials Research and Engineering (IMRE), 3 Research Link, Singapore 117602

Received: October 25, 2005; In Final Form: December 22, 2005

In this article, we report the synthesis of methylene-bridged periodic mesoporous organosilicas (PMOs) of the SBA-15 type. The materials were characterized by SAXS, BET, NMR, FESEM, and TEM. It was found that the synthesis of methylene-bridged SBA-15 PMOs requires more rigorous conditions than that of SBA-15 PMOs bearing organic bridges other than methylene. A mild acidic environment, which slows down the hydrolysis and condensation rates of the precursor, with the assistance of a salt, which enhances precursor−template interaction, should be used to synthesize high-quality large-pore methylene-bridged PMOs. We attributed this to the fast hydrolysis and condensation rates and the rigid backbone of precursor 1,2-bis(triethoxysilyl)methylene. By examining and comparing the synthesis of three large-pore PMOs with different bridges, we concluded that the inductive, bridging, and conformation effects of the organic bridging group play an important role in the synthesis of large-pore PMO materials.

Introduction

Surfactant-mediated synthesis[1] of periodic mesoporous organosilicas (PMOs) by hydrolysis and condensation of bridged silsesquioxanes $(RO)_3-Si-R'-Si-(RO)_3$ has attracted much interest recently.[2−15] With a sophisticated choice of the organic bridging groups R′, PMOs offer not only many desirable chemical properties, such as surface hydrophobicity, but also improved physical properties, such as stabilities,[16−18] thus having a greater application potential in catalysis,[19] adsorption,[20] and nanostructure templating[21] than the pure silica counterpart.

The MCM-41-type PMO materials with a 2-D hexagonal structure (*P*6*mm*) have been widely studied because of the relatively well-understood synthesis chemistry.[2−4] However, the small mesopore sizes of MCM-41 materials (2−6 nm) hinder the application development involving large molecules, such as proteins and organometallic complexes. Thus, PMO materials of the SBA-15 type[22] with larger pore sizes ranging from 6 to 30 nm are needed in many cases. However, the conventional synthesis recipes for SBA-15 periodic mesoporous silicas (PMSs), which employ strong acidic conditions,[22] do not yield high-quality SBA-15 PMOs.[5−7] Therefore, special synthesis techniques such as the true-liquid-crystal-templating method,[23] salt-assisted synthesis,[24] and solvent-assisted synthesis[25] have been exploited. In a recent study,[26] we have reported a low-acid-concentration synthesis strategy without involving any additives or using high concentration of template, by which high-quality ethylene- and ethynelene-bridged SBA-15 PMOs can be synthesized.

Methylene-bridged PMO is an important member of the PMO family from both the fundamental and application points of view.[16] Due to its simplicity, methylene is the only organic moiety that can be incorporated into microporous zeolites.[27] Methylene is also useful for subsequent chemical modifications. However, so far no report can be found in the literature on the synthesis of large-pore SBA-15 methylene-bridged PMOs.

In this work, the synthesis of high-quality methylene-bridged SBA-15 PMO was attempted. It has been identified that the synthesis of methylene-bridged SBA-15 PMOs is unique compared with that of SBA-15 PMSs and PMOs bearing organic functionalities other than methylene. The synthesis chemistry requests not only a controlled acid environment, which slows down the hydrolysis and condensation rates of the synthesis precursor, but also the aid of inorganic salt, which increases precursor−template interaction.[22,24] To understand the difference in the synthesis chemistry of SBA-15 PMOs bearing different organic functionalities, we have compared the synthesis of methylene-, ethylene-, and ethenylene-bridged SBA-15 PMOs with that of SBA-15 PMSs. It has been suggested that the inductive, bridging, and conformation effects of the different organic spacers R′ of silsesquioxanes $(RO)_3-Si-R'-Si-(RO)_3$ precursors are to be taken into account when designing and synthesizing SBA-15 PMOs.

Experimental Section

Chemicals and Synthesis. 1,2-bis(Triethoxysilyl)methylene (BTESM, 97%, Gelest), 1,2-bis(triethoxysilyl)ethylene (BTESE, 96%, Gelest), 1,2-bis(triethoxysilyl)ethenylene (BTESY, 95%, Gelest), tetraethyl orthosilicate (TEOS, 98%, Fisher), triblock copolymer $EO_{20}PO_{70}EO_{20}$ (Pluronic P123, Aldrich), fuming hydrochloric acid (HCl, 37%, Merck), and absolute ethanol (99.98%, Merck) were used as received.

In a typical synthesis, 0.5 g of P123 was dissolved in 7 mL of deionized water at 40 °C. An amount of 2.5×10^{-3} mol of BTESM was added in another solution of 1.2 mL of 1 M HCl in 7 mL of deionized water at 40 °C; 0.688 g of NaCl was added into the $Si/H_2O/HCl$ mixture if required. The $P123/H_2O$

* To whom correspondence should be addressed. E-mail: chezxs@nus.edu.sg.
[†] National University of Singapore.
[‡] Institute of Materials Research and Engineering.

10.1021/jp0561120 CCC: $33.50
Published on Web 01/21/2006

TABLE 1: Molar Compositions for Synthesizing ESM*y*, ESM*y*S, ESE*y*, ESY*y*, and OS*y* Materials

sample	Si	P123	HCl	H_2O	HCl/H_2O	NaCl
ESM1, ESE1 ESY1, OS1	1.00	0.0173	0.002	168	1.45×10^{-5}	0
ESM2, ESE2 ESY2, OS2	1.00	0.0173	0.048	168	2.86×10^{-4}	0
ESM3, ESE3 ESY3, OS3	1.00	0.0173	0.119	168	7.08×10^{-4}	0
ESM4, ESE4 ESY4, OS4	1.00	0.0173	0.243	168	1.45×10^{-3}	0
ESM5, ESE5 ESY5, OS5	1.00	0.0173	0.490	168	2.92×10^{-3}	0
ESM6, ESE6 ESY6, OS6	1.00	0.0173	3.773	168	2.25×10^{-2}	0
ESM1S	1.00	0.0173	0.002	168	1.45×10^{-5}	2.35
ESM2S	1.00	0.0173	0.048	168	2.86×10^{-4}	2.35
ESM3S	1.00	0.0173	0.119	168	7.08×10^{-4}	2.35
ESM4S	1.00	0.0173	0.243	168	1.45×10^{-3}	2.35
ESM5S	1.00	0.0173	0.490	168	2.92×10^{-3}	2.35
ESM6S	1.00	0.0173	3.773	168	2.25×10^{-2}	2.35

mixture was then transferred into the $Si/H_2O/HCl$ mixture slowly. The resulting gel was stirred for 24 h at 40 °C before being transferred into a polypropylene bottle and autoclaved at 100 °C for 120 h. The white solids were recovered by filtration, washed, and dried under ambient conditions. For comparison, ethylene-, ethenylene-bridged SBA-15 PMOs, and SBA-15 PMSs were also synthesized by the same method using BTESE, BTESY, and TEOS as the precursors, respectively. The molar ratios of HCl/H_2O were systematically varied in the range of 1.45×10^{-5} to 2.25×10^{-2}. The samples thus prepared are denoted as ESM*y*, ESE*y*, ESY*y*, and OS*y*, where ESM, ESE, ESY, and OS represent that the samples were prepared with BTESM, BTESE, BTESY, and TEOS as the precursors, respectively; *y* is an integer between 1 and 6, representing samples prepared at various HCl/H_2O ratios. The ESM*y* samples prepared in the presence of salt are denoted as ESM*y*S. Table 1 gives the names and the synthesis molar compositions of the samples. To remove P123, the as-synthesized materials and ethanol in a ratio of 1 g/300 mL were stirred at 60 °C for 6 h and the solids were recovered by filtration and air-dried.

Characterization. Small-angle X-ray scattering (SAXS) measurements were performed on a Bruker NanoStar at 40 kV and 35 mA with Cu Kα radiation of wavelength $\lambda = 1.54184$ Å. The distance between the sample and detector was 1.1 m. N_2 sorption isotherms were measured on a Quantachrome NOVA 1200 system at 77 K. Samples were degassed at 323 K for 2 h before measurements. Field-emission scanning electron microscopy (FESEM) images were obtained with a JEOL JSM-6700F microscope at an accelerating voltage of 5.0 kV. Transmission electron microscopy (TEM) images were collected on a JEOL 2010 electron microscope operated at an acceleration voltage of 200 kV. Solid-state magic-angle spinning (MAS) nuclear magnetic resonance (NMR) spectra were collected on a Bruker DRX400 MHz FT-NMR spectrometer with a MAS speed of 8 kHz. The cross-polarization (CP) technique was used for both the ^{13}C and ^{29}Si spectra, which were referenced to tetramethylsilane.

Results and Discussion

Synthesis and Characterization of Methylene-Bridged SBA-15 PMOs. The SAXS patterns of the ESM*y* materials synthesized under various acidic conditions without the presence of NaCl are displayed in Figure 1a. The peaks are assigned according to a 2-D hexagonal crystallographic structure with space group *P*6*mm*. It is seen that, unlike ethylene-bridged SBA-15 PMOs,[26] high-quality ESM*y* materials were not obtained within the acid concentration range studied as reflected by the broad (10) peak and the lack of higher order peaks. However, improvement on structural ordering, as shown by the increased SAXS peak sharpness with decreasing acid concentration, is still seen. No precipitate was formed after 24 h of stirring with acid concentrations equal or below that of ESM4 ($HCl/H_2O = 1.45 \times 10^{-3}$).

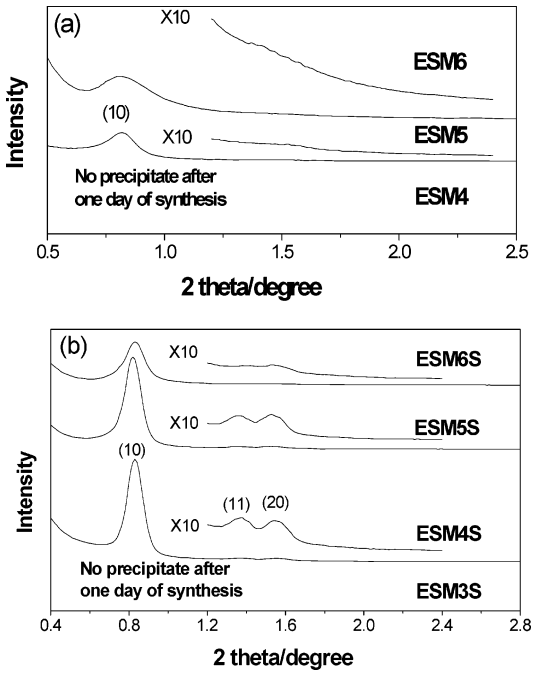

Figure 1. SAXS patterns of ESM*y* materials synthesized at various HCl/H_2O ratios in the absence (a) and presence (b) of NaCl salt.

In the presence of NaCl, better structured PMO materials were obtained as revealed by the SAXS patterns shown in Figure 1b. However, the material ESM6*y*S synthesized at a high HCl/H_2O ratio of 2.25×10^{-2} still displays a broad (10) peak. It is to be noted that this HCl/H_2O ratio is still much lower than that used for the synthesis of SBA-15 PMSs.[5-7] High-quality ESM*y* materials with a sharp (10) peak were only obtained in the systems with low acid concentrations as reflected by the SAXS patterns of samples ESM4S and ESM5S shown in Figure 1b. The SAXS patterns of the EMS*y*S materials synthesized in this work show that both a mildly acidic environment and the assistance of salt have to be present in order for the assembly of a well-structured methylene-bridged large-pore PMO.

The N_2 sorption isotherms of the ESM*y*S materials synthesized in the presence of NaCl are shown in Figure 2. All materials exhibit isotherms resembling type IV[28] with a nearly parallel hysteresis loop. This strongly suggests the presence of cylindrical pores opened at both ends in the materials, in accordance with the 2-D hexagonal pore structure revealed by the SAXS data. The isotherms of ESM6S synthesized with NaCl displays a large secondary hysteresis at high relative pressure ranges, probably due to the interparticle pores. Sharp capillary condensations and a reduction in secondary hystereses are seen from the N_2 sorption isotherms of ESM5S and EMS4S, suggesting uniform mesopores and large particle sizes. The total pore volumes, mesopore volumes, pore sizes, BET surface areas, and pore wall thicknesses of the materials calculated from their N_2 sorption isotherms and SAXS patterns are tabulated in Table 2. The mesopore volume was increased from 0.43 to 0.70 cm^3/g as the HCl/H_2O ratio was lowered from 2.25×10^{-2} (ESM6S)

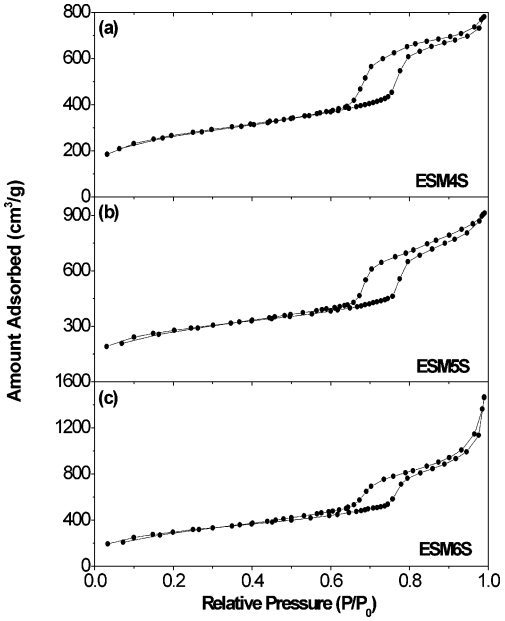

Figure 2. N_2 sorption isotherms of the ESM*y*S materials synthesized in the presence of NaCl.

TABLE 2: Structural Parameters of ESM*y*S Materials (Synthesized with NaCl) Determined from N_2 Adsorption Isotherms and SAXS Patterns

sample	MSE4S	MSE5S	MSE6S
D_{BJH} (nm)[a]	9.1	9.1	9.1
a[b]	12.3	12.4	12.3
t (nm)[c]	3.2	3.3	3.3
S_{BET} (m^2/g)[d]	893	961	1067
V_t (cm^3/g)[e]	1.21	1.41	2.27
V_{mes} (cm^3/g)[f]	0.70	0.68	0.43

[a] The pore sizes, D_{BJH}, were obtained from the peak positions of the BJH pore size distribution curves calculated from the adsorption branches of the isotherms. [b] The unit cell parameters, *a*, were calculated from the (10) peaks of the SAXS patterns. [c] Pore wall thicknesses, *t*, were calculated as a difference between the unit cell parameters, *a*, and the BJH pore sizes, D_{BJH}. [d] The specific surface areas, S_{BET}, were calculated by using the multiple-point Brunauer−Emmett−Teller (BET) method in the relative pressure range of $P/P_0 = 0.05-0.30$. [e] The total pore volumes, V_t, were calculated at a relative pressure of 0.99. [f] The mesopore volumes, V_{mes}, were calculated according to the α_s-plot method (ref 28).

to 1.45×10^{-3} (ESM4S), showing the benefit of employing a low HCl/H_2O ratio during synthesis.

The FESEM images of the ESM*y*S materials synthesized in the presence of NaCl are displayed in Figure 3. Aggregates of fine particles with sizes of about 100 nm are seen on sample ESM6S. The interparticle spaces resulting from the aggregation of the fine particles contribute to the large secondary hysteresis seen from the N_2 sorption isotherms. Both samples ESM5S and ESM4S exhibit ropelike macrostructures made up of bundles of fiberlike particles. A closer look at the fibers (Figure 3b) reveals that they have hexagonal cross sections, indicating that these fibers are single crystals with pore channels running parallel to the long axes of the fibers.[29] Therefore, materials ESM4S and ESM5S synthesized at relatively low HCl/H_2O ratios possess larger ordered domains than the ESM6S material synthesized at a higher HCl/H_2O ratio. The TEM images of sample ESM4S observed from different orientations, shown in Figure 4, confirmed the 2-D hexagonal pore structure with *P*6*mm* symmetry.

The solid-state ^{29}Si CP-MAS NMR spectrum of a representative material ESM4S (Figure 5a) displays three prominent

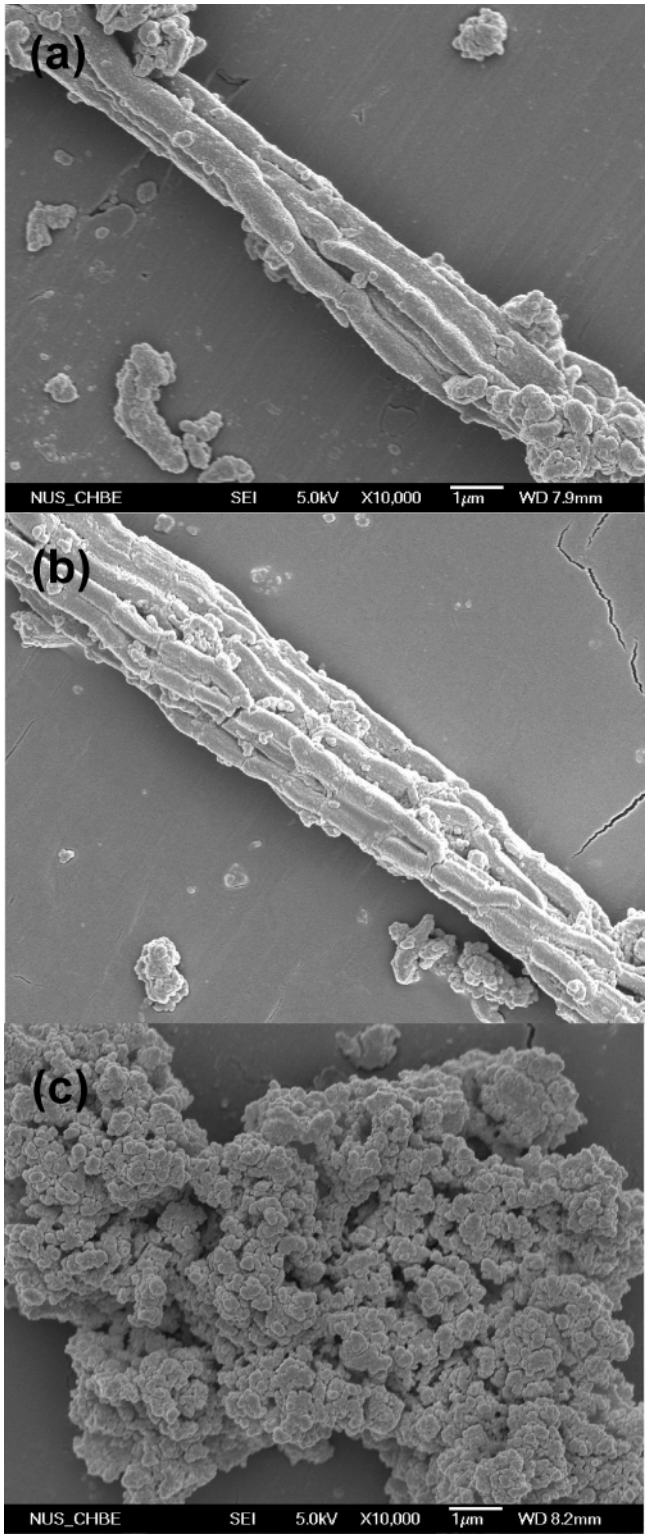

Figure 3. FESEM micrographs of the methylene-bridged SBA-15 PMOs synthesized at various HCl/H_2O ratios with NaCl: (a) ESM4S; (b) ESM5S; (c) ESM6S.

magnetic signals at −51, −61, and −69 ppm, which can be assigned to Si species covalently bonded to carbon atoms of T_1 [$SiC(OH)_2(OSi)$], T_2 [$SiC(OH)(OSi)_2$], and T_3 [$SiC(OSi)_3$], respectively.[26] No Q [$Si(OSi)_4$] silicon sites are seen, indicating that the Si−C bonds remained intact under the synthesis and subsequent processing conditions. The ^{13}C CP-MAS NMR spectrum of the sample depicted in Figure 5b shows a prominent signal at ~0 ppm, which corresponds to the methylene carbons.[16]

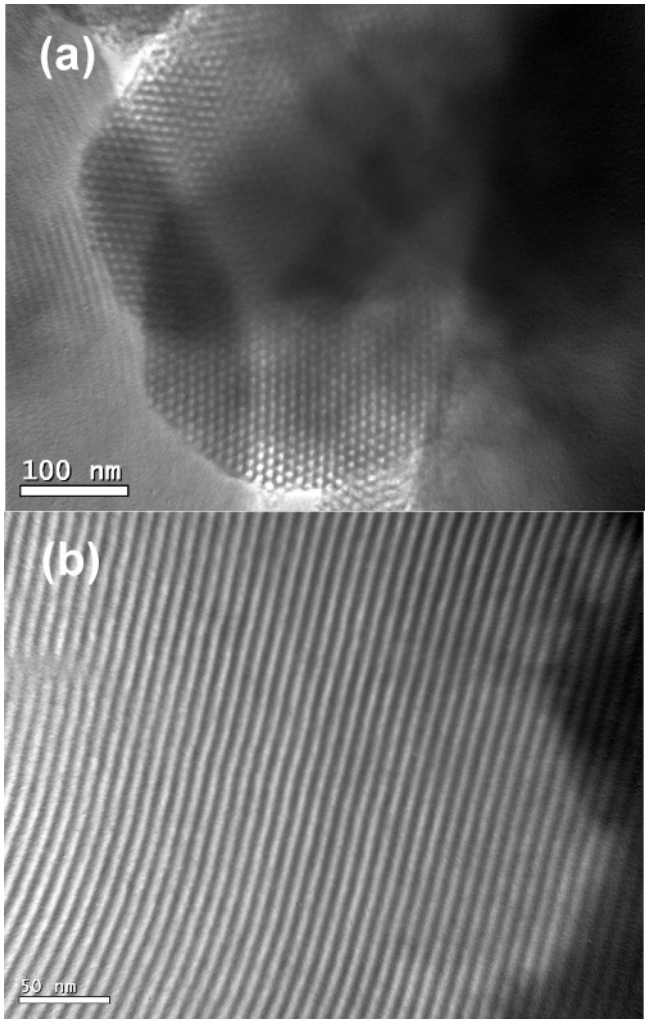

Figure 4. TEM micrographs of the ESM4S material synthesized with NaCl.

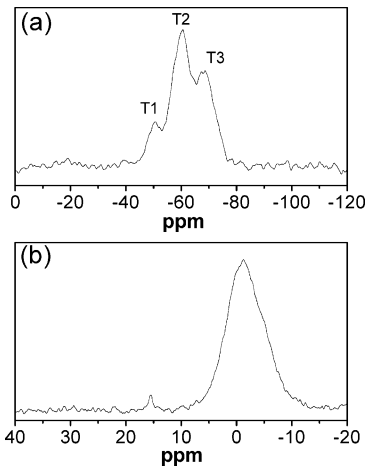

Figure 5. (a) ^{29}Si CP-MAS NMR and (b) ^{13}C CP-MAS NMR of ESM4S synthesized with NaCl after solvent extraction.

Comparison of the Syntheses of SBA-15 PMOs and PMSs. To understand the uniqueness of the synthesis of methylene-bridged SBA-15 PMOs, a series of synthesis experiments involving SBA-15 PMOs with other organic bridges and SBA-15 pure silicas were conducted and compared. The SAXS patterns of the ESE*y*, ESY*y*, and OS*y* materials synthesized under various acidic conditions are displayed in Figure 6. The peaks are assigned according to a 2-D hexagonal crystallographic structure with space group *P*6*mm*. It is seen that different SBA-15 PMOs and PMSs require different acid concentrations for precipitation and the formation of regular mesostructures. The acid concentration ranges, within which precipitation, irregular mesostructure formation, and regular mesostructure formation occurred for the SBA-15 PMO and PMS materials are summarized in Figure 7.

From Figures 6 and 7, it is seen that among the four materials investigated, regular mesostructures of OS*y* can be formed at the broadest HCl/H_2O ratio range, as shown by the white region in Figure 7, followed by the ESY*y*, ESE*y*, and ESM*y* materials. For example, well-ordered OS*y* materials can be formed at all HCl/H_2O ratios above 2.86×10^{-4}. However, well-structured ethenylene-bridged ESY materials can be obtained at all HCl/H_2O ratios above 2.86×10^{-4} but below 2.25×10^{-2}. Ethylene-bridged ESE material precipitated at a much narrower HCl/H_2O range, and its well-ordered structure could only be formed at HCl/H_2O ratios between 7.08×10^{-4} and 2.92×10^{-3}. Well-structured methylene-bridged ESM materials, on the other hand, could only be formed with the aid of an inorganic salt at a narrow HCl/H_2O range between 1.45×10^{-3} and 2.92×10^{-3}.

It is known that the inductive effect of the organic spacer and the steric effect of the alkoxy groups in a bridged silsesquioxane have significant impacts on its hydrolysis/condensation behaviors,[30,31] consequently the formation of PMO materials. While $-CH_2-$ and $-CH_2-CH_2-$ groups are weak electron donors, $-CH{=}CH-$ is a weak electron-withdrawing group; the $-OC_2H_5$ group, on the other hand, is strongly electron-withdrawing.[30,31] The electron-providing organic groups accelerate hydrolysis and condensation, while the electron-withdrawing organic groups retard hydrolysis and condensation. Since all of the silica/organosilica precursors used in this study bear ethoxy groups, the steric effect of the ethoxy groups on the hydrolysis/condensation of the silica/organosilica precursors is identical. Thus the hydrolysis and condensation rates of BTESM, BTESY, BTESE, and TEOS shall follow the sequence of BTESE > BTESM > BTESY > TEOS.

Other than the inductive effect, two additional effects, namely, the bridging effect and the conformation effect, are suggested to be taken into account when the hydrolysis and condensation behaviors of the organosilica precursors are discussed. When hydrolyzed, the bridging $-CH_2-$, $-CH_2-CH_2-$, and $-CH{=}CH-$ groups reduce the amount of $-OH$ group per Si compared with that of TEOS. This reduces the interaction between organosilica precursors and templates because the $-OH$ groups are primarily responsible for the interaction between the organosilica precursor and the template. The conformation effect refers to the conformational rigidity brought about by the organic spacers. While $Si-O-Si$ bonds are relatively flexible, $Si-CH_2-Si$, $Si-CH_2-CH_2-Si$, and $Si-CH{=}CH-Si$ bond angles are comparatively restricted; this is particularly true for $Si-CH_2-Si$ bonds,[11] in which the relative special position of the two Si atoms is fixed due to the tetracoordinated C atom. Both the bridging and conformation effects are adverse to the interactions between the hydrolyzed organosilica precursors and P123 template. The more rapid condensation rate due to the inductive effect and the weaker precursor−template interaction due to the bridging and conformation effects of the organosilica precursors require a small amount of acid, which is a catalyst for hydrolysis and condensation of the organosilicas,[30,31] to be used in order to slow the condensation rate, thus allowing a more thermodynamically favored coassembling process.[26] However, under very low acidic conditions, an ordered mesostructure cannot well develop not only because of the very slow condensation rate

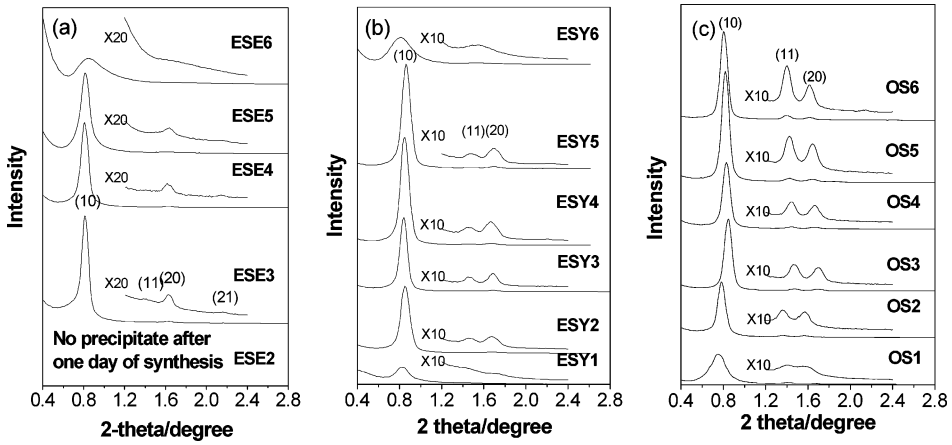

Figure 6. SAXS patterns of (a) ESE*y* materials, (b) ESY*y* materials, and (c) OS*y* materials synthesized at various HCl/H_2O ratios.

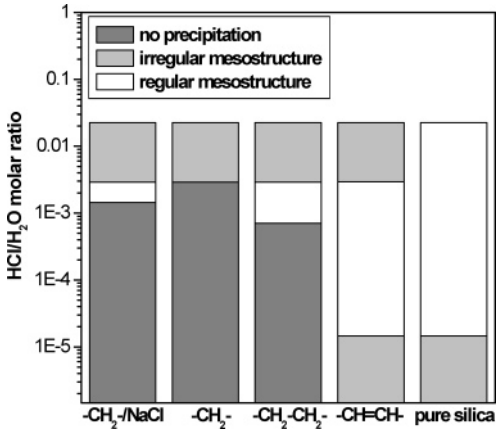

Figure 7. Schematic illustration of the HCl/H_2O ranges where irregular mesostructure, regular mesostructure, and no precipitation occurs for the SBA-15 PMOs and PMSs.

but also the lack of protonated hydroxyl groups, which are essential for the organosilicate−micelle coassembly.[26]

On the basis of the discussion above, the differences in the synthesis chemistries among the PMO materials and between the PMO and PMS materials can be understood. For example, although BTESE intrinsically hydrolyzes and condenses faster than TEOS, no precipitate was formed for the ESE*y* system within 24 h with $HCl/H_2O = 1.45 \times 10^{-5}$ (ESE1), while for the OS*y* system, a mesophase (OS1) was obtained under the same experimental conditions (Figure 6c). This is due to the bridging and conformation effects of BTESE, which, according to the discussions above, reduce the precursor−template interaction. It has been reported that the precursor−template interaction promotes intermolecular condensation.[26] Thus in the OS*y* system, precipitation can form at a very low acid concentration due to the stronger precursor−template interaction than that of the ESE*y* system.

On the other hand, the ESY*y* system, also suffering from the same bridging and conformation effects as the ESE*y* system does, can precipitate at $HCl/H_2O = 1.45 \times 10^{-5}$ (ESY1), despite the fact that BTSEY hydrolyzes and condenses at a slower rate than BTESE does. This suggests that the hydrolyzed BTSEY can interact with the surfactant micelles better than BTESE. This is probably related to the positive effect of the −CH═CH− bond in promoting the assembly of organosilicates and surfactant micelles. The π bond of an alkylene, as a nucleophile, could interact with $H_3{}^+O$ in solution, thus contributing to the interaction between the organosilicates and the micelles.[32]

In our experiment, high-quality ESM*y* was not obtained under any of the acid concentrations investigated without the presence of NaCl. In addition, no precipitation was formed even at an HCl/H_2O ratio as high as 1.45×10^{-3}, despite the fastest hydrolysis and condensation rates of BTESM among all three organosilica precursors. Nonetheless, improvement on structural ordering by decreasing acid concentration, as shown by the increased SAXS peak sharpness with decreasing acid concentration, can still be achieved (see Figure 1a). We propose that the difficulty in synthesizing SBA-15 methylene-bridged PMOs is largely due to the conformation effect of the $Si-CH_2-Si$ bond. The spacial rigidity of the Si atoms due to the tetracoordinated C atom, together with the bridging effect experienced by BTESM, lead to the weakest precursor−template interaction among the organosilica precursors studied in this work. The weak precursor−template interaction retarded the mesostructure precipitation despite of the rapid hydrolysis and condensation rates of its precursor. Inorganic salt is known to promote precursor−template interaction by decreasing the hydrophilicity of the PEO blocks of the surfactant micelles so that the low-hydrophilic PEO headgroups are able to interact better with the positively charged organosilane species with low hydrophilicity.[24] The addition of inorganic salt, together with the employment of a relatively low acid concentration, increased the hydrolyzed precursor−template interaction and slowed the condensation rate of the precursor, hence afforded a better structure (Figure 1b).

According to the above discussion, a generalized approach toward the synthesis of large-pore PMOs may be summarized. The first step is to identify the inductive, bridging, and conformation effects of an organic spacer. The objectives are to increase the hydrolyzed precursor−template interaction and/or to reasonably reduce the condensation rate of the hydrolyzed precursors. These can be achieved by measures such as adding an inorganic salt, which assists the precursor−template interaction,[24] reducing acid concentration[26] or adding an alcohol, which retards the rate of hydrolysis and condensation. Depending on the relative extent of the inductive, bridging, and conformation effects, sometimes only one measure may be considered, e.g., in the cases of ESE*y* and ESY*y* systems, while in other cases, more than one measure should be taken into account, e.g., the ESM*y* system.

Conclusions

In this article, the synthesis of high-quality methylene-bridged SBA-15 PMOs has been demonstrated. It is found that different from ethylene and ethenylene-bridged SBA-15 PMOs, high-

quality methylene-bridged SBA-15 PMOs can be obtained with both a mild acidic environment and the assistance of salt. To understand such difference, the syntheses of three SBA-15 PMOs with different organic spacers and pure silica SBA-15 were compared and evaluated. We propose that the rigorous conditions required for synthesizing methylene-bridged large-pore PMOs are due to the fast hydrolysis/condensation rates and the rigid backbone of the methylene precursor. Furthermore, based on the experiments, we propose that the inductive, bridging, and conformation effects of the organic spacers in the bridged silsesquioxanes are the factors determining the synthesis of SBA-15 PMOs and are the key parameters to be taken into consideration when future SBA-15 PMOs with new organic bridges are to be synthesized.

References and Notes

(1) Kresge, C. T.; Leonowicz, M. E.; Roth, W. J.; Vartuli, J. C.; Beck, J. S. *Nature* **1992**, *359*, 710.
(2) Inagaki, S.; Guan, S.; Fukushima, Y.; Ohsuna, T.; Terasaki, O. *J. Am. Chem. Soc.* **1999**, *121*, 9611.
(3) Melde, B. J.; Holland, B. T.; Blanford, C. F.; Stein, A. *Chem. Mater.* **1999**, *11*, 3302.
(4) Asefa, T.; MacLachlan, M. J.; Coombs, N.; Ozin, G. A. *Nature* **1999**, *402*, 867.
(5) Burleigh, M. C.; Markowitz, M. A.; Wong, E. M.; Lin, J. S.; Gaber, G. P. *Chem. Mater.* **2001**, *13*, 4411.
(6) Muth, O.; Schellbach, C.; Froba, M. *Chem. Commun.* **2001**, 2032.
(7) Cho, E. B.; Kwon, K. W.; Char, K. *Chem. Mater.* **2001**, *13*, 3837.
(8) Yang, Q. H.; Yang, J.; Liu, J.; Li, Y.; Li, C. *Chem. Mater.* **2005**, *17*, 3019.
(9) Matos, J. R.; Kruk, M.; Mercuri, L. P.; Jaroniec, M.; Asefa, T.; Coombs, N.; Ozin, G. A.; Kamiyama, T.; Terasaki, O. *Chem. Mater.* **2002**, *14*, 1903.
(10) Guo, W. P.; Kim, I.; Ha, C. S. *Chem. Commun.* **2003**, 2692.
(11) MacLachlan, M. J.; Asefa, T.; Ozin, G. A. *Chem.—Eur. J.* **2000**, *6*, 2507.
(12) Asefa, T.; Yoshina-Ishii, C.; MacLachlan, M. J.; Ozin, G. A. *J. Mater. Chem.* **2000**, *10*, 1751.
(13) Kickelbick, G. *Angew. Chem., Int. Ed.* **2004**, *43*, 3102.
(14) Inagaki, S.; Guan, S.; Ohsuna, T.; Terasaki, O. *Nature* **2002**, *416*, 304.
(15) Landskron, K.; Hatton, B. D.; Perovic, D. D.; Ozin, G. A. *Science* **2003**, *302*, 266.
(16) Asefa, T.; MacLachlan, M. J.; Grondey, H.; Coombs, N.; Ozin, G. A. *Angew. Chem., Int. Ed.* **2000**, *43*, 1808.
(17) Burleigh, M. C.; Markowitz, M. A.; Jayasundera, S.; Spector, M. S.; Thomas, C. W.; Gaber, B. P. *J. Phys. Chem. B* **2003**, *107*, 12628.
(18) Lu, Y.; Fan, H.; Doke, N.; Loy, D. A.; Assink, R. A.; LaVan, D. A.; Brinker, C. J. *J. Am. Chem. Soc.* **2000**, *122*, 5258.
(19) Bhaumik, A.; Kapoor, M. P.; Inagaki, S. *Chem. Commun.* **2003**, 470.
(20) Burleigh, M. C.; Markowitz, M. A.; Spector, M. S.; Gaber, B. P. *Environ. Sci. Technol.* **2002**, *36*, 2515.
(21) Sakamoto, Y.; Fukuoka, A.; Higuchi, T.; Shimomura, N.; Inagaki, S.; Ichikawa, M. *J. Phys. Chem. B* **2004**, *108*, 853.
(22) Zhao, D.; Huo, Q.; Feng, J.; Chmelka, B. F.; Stucky, G. D. *J. Am. Chem. Soc.* **1998**, *120*, 6024.
(23) Zhu, H. G.; Jones, D. J.; Zajac, J.; Roziere, J.; Dutartre, R. *Chem. Commun.* **2001**, 2568.
(24) Guo, W. P.; Park, J. Y.; Oh, M. O.; Jeong, H. W.; Cho, W. J.; Kim, I.; Ha, C. S. *Chem. Mater.* **2003**, *15*, 2295.
(25) Wang, W.; Xie, S.; Zhou, W. Sayari, A. *Chem. Mater.* **2004**, *16*, 1756.
(26) Bao, X. Y.; Zhao, X. S.; Li, X.; Chia, P. A.; Li, J. *J. Phys. Chem. B* **2004**, *108*, 4684.
(27) Yamamoto, K.; Sakata, Y.; Nohara, Y.; Takahashi, Y.; Tatsumi, T. *Science* **2003**, *300*, 470.
(28) Gregg, S. J.; Sing, K. S. W. *Adsorption, Surface Area and Porosity*; Academic Press: London, 1982.
(29) Bao, X. Y.; Zhao, X. S. *J. Phys. Chem. B* **2005**, *109*, 10727.
(30) Brinker, C. J. *J. Non-Cryst. Solids* **1988**, *100*, 31.
(31) Hook, R. J. *J. Non-Cryst. Solids* **1996**, *195*, 1.
(32) Loy, D. A.; Shea, K. J. *Chem. Rev.* **1995**, *95*, 1431.